



*Citation for published version:*

Wain, DJ, Lilly, JM, Callaghan, AH, Yashayaev, I & Ward, B 2015, 'A breaking internal wave in the surface ocean boundary layer', *Journal of Geophysical Research : Oceans*, vol. 120, no. 6, pp. 4151-4161.  
<https://doi.org/10.1002/2014JC010416>

*DOI:*

[10.1002/2014JC010416](https://doi.org/10.1002/2014JC010416)

*Publication date:*

2015

*Document Version*

Peer reviewed version

[Link to publication](#)

## University of Bath

### General rights

Copyright and moral rights for the publications made accessible in the public portal are retained by the authors and/or other copyright owners and it is a condition of accessing publications that users recognise and abide by the legal requirements associated with these rights.

### Take down policy

If you believe that this document breaches copyright please contact us providing details, and we will remove access to the work immediately and investigate your claim.

# A breaking internal wave in the surface ocean boundary layer

Danielle J. Wain<sup>1,2</sup>, Jonathan M. Lilly<sup>3</sup>, Adrian H. Callaghan<sup>1,4</sup>, Igor Yashayaev<sup>5</sup>, and Brian Ward<sup>1</sup>

---

Corresponding author: B. Ward, School of Physics, National University of Ireland, Galway, Ireland. (bward@nuigalway.ie)

<sup>1</sup>School of Physics, National University of Ireland, Galway, Ireland.

<sup>2</sup>Now at Department of Architecture and Civil Engineering, University of Bath, UK.

<sup>3</sup>NorthWest Research Associates, Redmond, WA 98052, USA.

<sup>4</sup>Scripps Institution of Oceanography, University of California, San Diego, La Jolla, California, USA.

<sup>5</sup>Bedford Institute of Oceanography, B2Y 4AZ, Dartmouth, Nova Scotia, Canada.

This article has been accepted for publication and undergone full peer review but has not been through the copyediting, typesetting, pagination and proofreading process which may lead to differences between this version and the Version of Record. Please cite this article as doi: 10.1002/2014JC010416

© 2015 American Geophysical Union  
Received: Aug 31, 2014; Revised: May 02, 2015; Accepted: May 07, 2015

**Abstract.** High-temporal resolution measurements in the Labrador Sea surface layer are presented using an upwardly-profiling autonomous microstructure instrument, which captures an internal wave in the act of breaking at the base of the surface mixed layer, driving turbulence levels two to three orders of magnitude above the background. While lower-frequency (near-inertial) internal waves are known to be important sources of turbulence, we report here a higher frequency internal wave breaking near the ocean surface. Due to observational limitations, the exact nature of the instability cannot be conclusively identified, but the interaction of wave-induced velocity with unresolved background shear appears to be the most likely candidate. These observations add a new process to the list of those currently being considered as potentially important for near-surface mixing. The geographical distribution and global significance of such features is unknown, and underscores the need for more extensive small-scale, rapid observations of the ocean surface layer.

## 1. Introduction

The ocean surface mixed layer is a critical interface for air-sea interaction. The physical processes controlling turbulent mixing within the ocean surface mixed layer impact the air-sea exchange of momentum, heat, and carbon dioxide, and also set the properties of ventilated water masses that eventually subduct into the ocean interior. For these reasons, global climate models are known to be sensitive to parameterizations of near-surface turbulent mixing [Fox-Kemper *et al.*, 2011; Belcher *et al.*, 2012], as this modulates the mixed layer depth [Stevens *et al.*, 2011].

Higher-frequency internal waves in the upper ocean have been shown to be a source of turbulence, mixing, and vertical heat fluxes through the pycnocline [Barton *et al.*, 2001; Dewey *et al.*, 1999]. Away from topography, such waves can be generated in a variety of ways, most of which originate with input of wind energy into the mixed layer. Inertial motions can excite a wide spectrum of internal waves, from low mode near-inertial waves that can propagate far from their generation site to higher-frequency waves which dissipate locally [Bell, 1978; Simmons and Alford, 2012]. Perturbations on the base of mixed layer from Langmuir cells [Polton *et al.*, 2008; Belcher *et al.*, 2012], nighttime convection [Wijesekera and Dillon, 1991; Ansong and Sutherland, 2010], shear instabilities [Lien *et al.*, 2002; Dohan and Davis, 2011], and turbulent patches [Dohan and Sutherland, 2003] can all generate internal waves with frequencies near the buoyancy frequency  $N$ . These waves can transfer energy from the mixed layer and through the transition layer—the highly stratified region at the base of the surface mixed layer—to the pycnocline, where they remain trapped because they cannot propagate through the weakly stratified

region below the pycnocline [Johnston and Rudnick, 2009]. These waves can then break and generate turbulence through self-induced shear or steepening through interactions with lower frequency waves or background shear [Thorpe, 2005]. The relative importance of these various processes is not yet known, with observational challenges being recognized as a limiting factor [Belcher et al., 2012; Sutherland et al., 2014].

Near-surface mixing processes take on a particular significance in the Labrador Sea, a region of the North Atlantic's subpolar gyre that is one of the key locations for the Atlantic Meridional Overturning Circulation (AMOC). There, intense wintertime cooling leads to deep convection to depths of 500–2000 m, forming a mode water known as Labrador Sea Water [e.g. Lilly et al., 1999]. Each spring, a rapid surface freshening is observed across the Labrador Sea basin [Lilly et al., 1999; Straneo, 2006; Schmidt and Send, 2007], resulting in a 200–300 m thick highly buoyant layer that serves as a barrier to the next winter's deep convection. The predictability of deep water ventilation in the Labrador Sea requires understanding not only of the variability in the wintertime surface heat loss, but also the near-surface processes that contribute to rebuilding a stable stratification [Våge et al., 2009]. While this rapid surface capping appears to be a generic feature of convective regions [Marshall and Schott, 1999], little is known about its dynamics. With freshwater discharge from the Arctic now dramatically increasing [Peterson et al., 2006], it is important to understand Labrador Sea surface processes at work during restratification.

Motivated by the importance of near-surface mixing in general, and in deep convection regions in particular, the first direct microstructure turbulence measurements from the Labrador Sea were collected during May 2010. These were obtained using the Air-Sea Interaction Profiler (ASIP), an autonomous, upwardly-profiling instrument [Ward et al.,

2014; *Sutherland et al.*, 2014; *Callaghan et al.*, 2014; *Sutherland et al.*, 2013]. This instrument is specifically designed to make high-resolution microstructure profiles of the ocean surface layer, a climatically important region of the ocean for which very few direct microstructure measurements are available. Other microstructure platforms typically profile downward starting from a depth of tens of meters, and focus on interior turbulence with temporal resolutions of 30 minutes or more. This dataset therefore provides a rare, high-resolution view into rapidly evolving near-surface dynamics.

The main result is the presentation of a breaking internal wave at the base of the Labrador Sea mixed layer. This adds a new candidate to the list of potential sources of upper-ocean turbulence, and offers a counterexample to other works [see e.g. *Johnston and Rudnick*, 2009] that identify near-inertial shear as the primary driver.

## 2. Observations

During May 2010, microstructure measurements of the Labrador Sea surface layer were collected as a part of a hydrographic cruise carried out annually by the Bedford Institute of Oceanography (BIO). Since 1990, BIO has repeatedly occupied the AR7W line of stations that stretches from the coast of Labrador to the coast of Greenland [e.g., *Lazier et al.*, 2002; *Yashayaev*, 2007; *Yashayaev and Loder*, 2009], as shown in Figure 1. Conductivity-temperature-depth (CTD) profiles of the upper water column along this section, see Figure 2, reveal a thin, 30–60 m buoyant layer over a largely unstratified interior. This structure is typical of the springtime Labrador Sea, a consequence of rapid freshwater restratification following deep convection [*Lilly et al.*, 1999; *Straneo*, 2006; *Schmidt and Send*, 2007].

A full-depth ( $\sim 3500$  m) CTD profile taken contemporaneously with the microstructure measurements describes the hydrographic background, see Figure 3. The buoyancy frequency  $N$  was computed by first completing a piecewise fit to the observed potential density  $\sigma_0$  profile, consisting of 14 linear segments above an exponential decay from 230 m to the bottom. This approach seemed to offer the best balance between preserving sharp gradients, while still averaging over small-scale noise. An accurate estimation of  $N$  allows us to determine the depth range over which internal waves will be trapped.

This CTD profile reveals a relatively warm, fresh surface layer about 60 m thick, above a weakly stratified interior with a buoyancy frequency of about  $N = 0.66$  cycles per hour (cph), or one cycle per 90 minutes (Figure 3). The transition layer—the highly stratified region between the well-mixed surface layer and the deep stratification—was roughly 10 m thick, with a peak buoyancy frequency of  $N = 6.6$  cph, an order of magnitude higher than weak interior value. For comparison, the inertial frequency at this latitude is 0.07 cph, or one cycle per 14.4 hours.

In addition, a shipboard Acoustic Doppler Current Profiler (ADCP), a Teledyne RDI Ocean Surveyor II 75kHz, recorded five minute averages of horizontal velocities in 8 m bins between 20 m and 650 m depth, see Figure 3b. Even taking the mean across the four hour time series, we found that 40 m averaging in the vertical was necessary to reduce noise. As a result of this temporal and vertical averaging, the resolvable shear is quite weak, around  $0.02 \text{ m s}^{-1}$  per 100 m over the depth interval containing the transition layer.

The microstructure data was acquired with ASIP, a 2.5 m long upward-profiling instrument that is outfitted with two shear probes, fast response conductivity and temperature (C/T) microstructure sensors, and slower more accurate C/T sensors. ASIP is unteth-

ered and profiles autonomously from as deep as 100 m to the sea surface. The instrument submerges itself to a preset depth using thrusters, and subsequently rises under its own buoyancy until it penetrates the surface. The rapid profiling capability of ASIP allows for processes with short time scales to be observed [see also *Sutherland et al.*, 2013].

On May 22, 2010, in the vicinity of the hydrographic profile shown in Figure 3, a 4-hour microstructure dataset was acquired using ASIP. During the deployment, ASIP drifted at about  $0.15 \text{ m s}^{-1}$  to the southeast, see Figure 4. The dataset consisted of 30 profiles of high-resolution temperature, conductivity, and velocity shear from 100 m to the surface, with approximately eight minutes between each profile, as presented in Figure 5.

The temperature and conductivity data from ASIP were averaged in half-meter vertical bins, after which salinity, density, and buoyancy frequency were computed following *McDougall and Barker* [2011]. Profiles were smoothed with 10 m running means before gradients were computed, for example, in the calculation of the buoyancy frequency presented in the upper panel of Figure 5. The mean density profile from ASIP is shown in Figure 3b for comparison with the CTD cast. The pycnocline is sharper in the CTD cast, as the 10-m amplitude oscillations in the pycnocline (discussed in detail below) broaden the density gradient in the ASIP profiles upon averaging.

The turbulent dissipation  $\epsilon$  was estimated from the shear power spectra using standard methods [*Yamazaki and Osborn*, 1990; *Oakey*, 1982]. The spectra were calculated over windows of 1000 points in length, corresponding to 0.5 s of sampling. The windows were shifted in 500 point intervals ensuring 50% overlap between adjacent  $\epsilon$  estimates, resulting in 0.25 m vertical bins for dissipation rate. Following *Osborn* [1980], the vertical eddy diffusivity  $K_\rho$  was then estimated from turbulent dissipation by assuming a balance



between mechanical production, buoyancy flux, and turbulent dissipation in the turbulent kinetic energy equation. This leads to a vertical eddy diffusivity given by  $K_\rho = \Gamma\epsilon/N^2$ , where the coefficient  $\Gamma$  is a mixing efficiency that is conventionally taken to be 0.2.

### 3. Results and Discussion

The displacement of the pycnocline seen in Figure 5a clearly reveals the presence of an internal wave, with a frequency of about 1.2 cph, or a 50 minute period, and large-amplitude isopycnal excursions of about 10 m in the vertical. Associated with these displacements is a patch of elevated turbulent dissipation at the base of the mixed layer between 45 and 55 m depth, indicated by the boxes in both panels of Figure 5, within which the dissipation rate  $\epsilon$  reached values as high as  $2 \times 10^{-7} \text{ m}^2 \text{ s}^{-3}$ . The deep patch of elevated dissipation is separated from the surface dissipation by a  $\sim 20$  m thick layer of very weak dissipation, with  $\epsilon$  values as low as  $\epsilon \sim 2 \times 10^{-10} \text{ m}^2 \text{ s}^{-3}$ . Therefore it appears clear that this patch is associated with the internal wave itself, rather than with turbulence-generating mechanisms at the surface. These enhanced dissipation rates approach the values associated with near-surface mixing, with peak values of  $\epsilon \sim 1 \times 10^{-6} \text{ m}^2 \text{ s}^{-3}$ , which are driven by surface heat losses and extend to roughly 30 m depth.

Until 19:44 UTC (Figure 5), the depth-averaged dissipation rate near the base of the mixed layer (between depths of 45 and 55 m) was low, averaging  $7 \times 10^{-10} \text{ m}^2 \text{ s}^{-3}$  over the first 10 profiles, which corresponds to a vertical turbulent eddy diffusivity of  $6 \times 10^{-6} \text{ m}^2 \text{ s}^{-1}$ . Between 19:44 and 21:02, during the patch of elevated turbulence, the depth-averaged dissipation rate exceeded  $2 \times 10^{-8} \text{ m}^2 \text{ s}^{-3}$ , with an average over these 10 profiles of  $1 \times 10^{-8} \text{ m}^2 \text{ s}^{-3}$ . The eddy diffusivity computed from the averaged dissipation profile during this time was elevated to  $1 \times 10^{-4} \text{ m}^2 \text{ s}^{-1}$ , with a maximum value of

$6 \times 10^{-4} \text{ m}^2 \text{ s}^{-1}$ , two orders of magnitude above the background values. After 21:02, the mean depth-averaged dissipation rate of the last 10 profiles dropped to  $3 \times 10^{-9} \text{ m}^2 \text{ s}^{-3}$ , which was still elevated above the background values, and which appeared at that time to detach vertically from the pycnocline base. At this same time, the turbulence from the surface begins penetrating to the depth of the pycnocline, perhaps due to convective overturns which lead to the observed statically unstable density field.

Wave speed and wavelength were estimated in two different ways, using different assumptions, both giving similar results. The first approach attempts to match the observed vertical distribution of isopycnal displacements with a suitable vertical mode. Vertical structure functions (which are independent of frequency) for the vertical modes were computed from the full-depth density profile using standard methods [e.g. *Gill*, 1982], and the upper 600 m of these structure functions are shown in Figure 3d. The shallowest extremum in vertical displacement amplitude for each mode was at 1892 m, 823 m, 295 m, 104 m, and 67 m, for modes 1–5, respectively. The internal wave captured by ASIP has a peak vertical displacement amplitude at 70 m, which is best matched by the extremum in mode five. The wave speed for this mode is  $0.28 \text{ m s}^{-1}$ ; for the observed frequency of wave, this corresponds to a horizontal wavenumber  $k = \omega/c = 0.0075 \text{ rad m}^{-1}$  or a horizontal wavelength of 840 m.

Alternatively, assuming that the wavelength is long compared to the depth of the surface layer, we can idealise the observed internal wave as an interfacial wave between a shallow surface layer and an infinitely deep lower layer. The long wave approximation can then be used to estimate the wave speed [see *Kundu and Cohen*, 2002] as  $c = \sqrt{g'H}$ , where  $g'$  is the reduced gravity  $g' = (\Delta\rho/\rho_o)g$ ,  $\Delta\rho$  is the density change over the interface,

$\rho_o$  is a reference density of  $1027 \text{ kg m}^{-3}$ , and  $H$  is the thickness of the surface layer, which here was chosen to be 60 m based on the average mixed layer depth from the ASIP measurements. In this calculation,  $\Delta\rho$  was computed as the difference between  $\sigma_0$  above and below the pycnocline. From the measurements,  $g'$  was found to be about  $0.002 \text{ m s}^{-2}$ , again yielding a phase velocity of  $0.3 \text{ m s}^{-1}$ ; thus both approaches lead to the same approximate estimate of the wave speed and wavelength of the waves observed here.

Due to the Labrador Sea's weak interior stratification, a wave of this frequency will be strongly trapped in the upper water column. The white lines in Figure 2 mark a buoyancy frequency of  $N = 1.2 \text{ cph}$ , indicating that the wave cannot exist below about 200 m at the ASIP measurement location. To further examine this trapping, the results of a ray tracing calculation are also shown in Figure 2. This ray tracing considered only  $N$  and not velocity shear, a standard approach which should be a good approximation in the Labrador Sea interior, away from strong currents. The weak stratification in the Labrador Sea basin after convection acts as a waveguide, confining waves at this frequency to the uppermost 100–300 m over this 300 km section. Thus the observed waves must have been generated by surface forcing of some type, as opposed to a deep source such as tidal interaction with bathymetry. Because of the strong waveguide, the horizontal location of the wave's origin cannot be identified, and in particular, a nonlocal origin is a distinct possibility. But the observed turbulent event here implies that horizontal propagation will be limited as energy is drained from the internal wave during breaking.

Based on the estimates above, we can attempt to use the available data to shed light on possible breaking mechanisms. A number of process could conceivably lead to the

breaking of an internal wave. An internal wave itself can generate convective instabilities or shear instabilities that lead to breaking. For a monochromatic wave in a fluid with an interface of finite thickness, *Fringer and Street* [2003] numerically showed how the required steepness for breaking depends upon the non-dimensional interface thickness  $\delta k$ , where  $\delta$  is a measure of the interface thickness defined in *Fringer and Street* [2003] and  $k$  is the horizontal wavenumber. The amplitude  $a$  of the waves here is approximately 10 m and  $\delta$  is 35 m. For the wave parameters estimated above, the  $ak$  is 0.075 and  $\delta k$  is 0.26. *Fringer and Street* [2003] found convective overturns for  $\delta k$  greater than 2.33 and  $ak$  greater than 1, thus such instabilities are not likely to play a role here.

Below  $\delta k = 2.33$ , shear instabilities were the observed breaking mechanism; the bottom end of the parameter range in *Fringer and Street* [2003] was  $\delta k = 0.31$ . The laboratory experiments of *Troy and Koseff* [2005] investigate breaking interfacial waves at non-dimensional thicknesses smaller than this, which are typical of longer waves, as observed here. They found that breaking occurred at a critical wave steepness  $ak_c = \sqrt{(2\delta k)}$ , where here  $ak_c$  is 0.72, an order of magnitude larger than the measured  $ak$ . Thus the waves are not inherently steep enough to break without the presence of shear from other sources [*Thorpe*, 1978].

Interaction with background shear could lead to wave breaking. Between 44 and 55 m, where the breaking occurs,  $N = 0.0042 \text{ rad s}^{-1}$ ; the change in velocity over this depth necessary to reduce the Richardson number below 1 is  $0.046 \text{ m s}^{-1}$ . To first order, the wave-induced velocity  $u_w$  can be approximated as  $a\omega$  [*Thorpe*, 2005]. The amplitude here is approximately 10 m, leading to an estimate of  $u_w = 0.021 \text{ m s}^{-1}$ . If the shear used in computing the Richardson number is the sum of the background shear and the wave

induced shear ( $du/dz \sim \Delta U/\delta + a\omega/\delta$ ), this wave-induced velocity enhanced by modest background shear would be sufficient to induce breaking; the velocity difference needed here is about  $0.025 \text{ m s}^{-1}$ .

Shipboard ADCP data is available during the time of the ASIP deployment. Thirty minute average ADCP velocity profiles are shown in Figure 6 without any vertical smoothing. The velocities in the surface mixed layer ( $0.15\text{--}0.20 \text{ m s}^{-1}$ ) are about an order of magnitude larger than the required velocity difference. The magnitude of variance is high, and is of the same order as the velocity difference needed to induce turbulence. However, after carrying out the processing that is necessary to reduce noise, with a five minute temporal average and 40 m smoothing, we find far lower values of the shear. There is, however, an observed acceleration of background environment by  $0.05\text{--}0.1 \text{ m/s}$  at the time of the elevated turbulence, suggesting that an unresolved change in the shear at this time is not implausible.

Thus the physical mechanism responsible for the elevated turbulence levels cannot be conclusively identified using the available data. Based on theoretical and laboratory based parameterisations, instabilities are not predicted, but the isopycnals appear to be vertical at the crest of the wave (Figure 5b). A reasonable explanation is that the background shear is under-represented by the shipboard ADCP measurements, as these data are more limited in their resolution than are ASIP's high-resolution measurements of the wave properties. This blurring of vertical gradients due to the averaging employed could have also obscured the required shear for generating Kelvin-Helmholtz instabilities (or potentially Holmboe instabilities if the maximum shear and density gradient are not co-located, e.g. *Smyth and Winters [2003]*). This difficulty is not unique to our dataset;

other authors have faced similar difficulties in identifying the source of shear instabilities using ADCP velocity data [Moum *et al.*, 2003].

Because of the issues surrounding estimating small scale velocity shear with shipboard ADCPs, we used the isopycnal displacements as measured by ASIP to estimate the fine-scale velocity structure following Moum *et al.* [2003]. In this approach, the velocity profile is inferred from the density profile by assuming that in the wave's frame of reference that the streamlines are parallel to the isopycnals and thus the velocity along each isopycnal can be estimated. See Moum *et al.* [2003] for further details. The isopycnal separation ( $\Delta\rho = 0.04 \text{ kg m}^{-3}$  in the current dataset) was chosen to remove fluctuations due to turbulence so that the remaining density profile is composed of the background profile and the wave. While coarsely resolved, the background velocity profile was taken to be the average profile from the ADCP and was relatively constant within the upper 100 m ( $0.18 - 0.20 \text{ m s}^{-1}$ ). The background density profile was taken as the mean density profile from the deployment. This method is valid until the turbulent event, after which it cannot be determined if the straining of isopycnals is from the wave or from mixing.

Using the highlighted isopycnals in Figure 5, the fine scale velocity structure was inferred for the first ten profiles of the deployment. The velocity profile from Profile 10 (19:43) is shown in Figure 7, where the isopycnals are compressed relative to the background profile, generating a shear layer in the the pycnocline. Note that the irregular spacing between data points is due to the use of isopycnal coordinates for this calculation. The sharp drop at the base of the mixed layer does appear to be a real feature, and is comparable to those observed in Moum *et al.* [2003] Figure 18.

From the velocities estimated here along the highlighted isopycnals, the Richardson number between the 2nd and 3rd isopycnals (where the turbulence is initiated) drops below 0.1 in the trough of the wave at Profile 8 (19:29) where the first observations of elevated turbulence are seen (Figure 5). The Richardson number then drops below 0.01 at Profile 10. This satisfies the more stringent Richardson number criterion of *Barad and Fringer* [2010], although with the existing dataset we are unable to determine if the length of time that the fluid is subjected to this low Richardson number is consistent with the growth rate of the instabilities. This has been found to play an important role in the breaking of interfacial waves in the laboratory [*Troy and Koseff*, 2005; *Barad and Fringer*, 2010]. While there are many assumptions in the approach taken here, the results indicate that finescale velocity from the wave passing through the ambient velocity field might be sufficient to initiate instability and thus turbulence. Once the turbulence is initiated, there is clear straining of the isopycnals after the crest of the wave, which has been associated with turbulent overturns in other environments [*Alford and Pinkel*, 2000] and thus might contribute to sustaining the turbulence.

While oscillations of the mixed layer base are commonly observed, well-resolved measurements of such higher-frequency internal waves are rather rare. One study that has previously reported on a similar wave, *Joyce and Stalcup* [1984], used acoustic observations to identify a 10 m amplitude, 10 minute period oscillation of the stratification below the mixed layer; their Figure 5 appears strikingly similar to the upper panel of our Figure 5. The stratification in that study, within a warm core ring, was described as consisting of a buoyant surface layer above a homogeneous water mass, separated by a strong

thermocline at 45 m. Thus these observations occurred in a similar surface-intensified stratification to that of the post-convection Labrador Sea.

An outstanding mystery is the mechanism or mechanisms responsible for generating these waves. As described in the introduction, there are several possible mechanisms that could account for local generation of high-frequency waves, but it is not clear which if any of these is the most likely. Earlier in the cruise, the central Labrador Sea experienced several days of strong winds (Figure 8) and attendant long-period swell, an energetic environment that would seem readily capable of giving rise to internal waves. In a recent review paper, *Polzin and L'vov* [2011, see their Section 5.3.2] point out that surface wave/internal wave coupling has been previously regarded primarily as a *sink* of internal wave energy. One might conjecture that swell could interact efficiently with a shallow stratification, along the lines of the well-known ‘dead water’ phenomenon of ship drag from interfacial waves in fjords [see e.g. *Gill*, 1982, Section 6.2]. However, *Polzin and L'vov* [2011] state, “rapid transfers of energy from a narrowband ocean swell to the internal wavefield are possible ... and remain to be quantified,” thus it appears that little is known about this possible wave source.

#### 4. Conclusions

Microstructure measurements from the Labrador Sea in May 2010 show a 10 m amplitude internal wave train, with a 50 minute period, associated with elevated levels of turbulence in the surface mixed layer. The breaking internal wave event observed here increased the average turbulent dissipation rate in the pycnocline from  $7 \times 10^{-10} \text{ m}^2\text{s}^{-3}$  to  $1 \times 10^{-8} \text{ m}^2\text{s}^{-3}$  and the average vertical eddy diffusivity from  $6 \times 10^{-6} \text{ m}^2\text{s}^{-1}$  to  $1 \times 10^{-4} \text{ m}^2\text{s}^{-1}$ , with maximum values of  $2 \times 10^{-7} \text{ m}^2\text{s}^{-3}$  and  $6 \times 10^{-4} \text{ m}^2\text{s}^{-1}$  respectively. The eddy



diffusivity is higher than the values estimated through internal wave parameterisations by *Lauderdale et al.* [2008] near the bottom of the central basin of the Labrador Sea and on par with those estimated in the same way by *Walter et al.* [2005] at mid-depths in the central basin, but in the latter study the elevated mixing was due to reduced stratification, not enhanced turbulence.

While observational limitations prevent us from identifying the exact breaking mechanism observed here, interaction of the internal wave and background shear appears to be the most likely candidate. These results appear to be the direct evidence that breaking internal waves may play a role in driving near-surface turbulence. This raises the question as to how widespread such features may be. With a profile interval of 5–10 minutes, ASIP's sampling rate is far higher than most other observational platforms, and its ability to profile upward to the sea surface is rare among microstructure instruments. Thus, even if such the breaking of internal waves at the mixed layer base are a commonplace occurrence, few of the standard oceanographic measurement platforms would be able to capture them. It is conceivable that such phenomenon are widespread but been overlooked due to observational limitations. Another possibility is that the occurrence of such a wave in the Labrador Sea is a particular consequence of the highly surface-intensified nature of the stratification in this region. If so, one may expect to find such waves in other regions with similar surface-intensified stratifications, such as the Gulf of Lion, Greenland Sea, and other regions of deep convection [*Marshall and Schott*, 1999]. Additional work is necessary to determine whether shallow dissipation by such waves may play a significant role in the restratification process following deep convection.

Processes such as mixing due to near-inertial shear [*Dohan and Sutherland, 2003*], and high-frequency wave generation associated with Langmuir cells [*Polton et al., 2008*], are already recognized as important processes in near-surface mixing. Recently, *Belcher et al. [2012]* showed that current surface turbulence parameterizations lead to biases in coupled climate models, a fact that they argued was due in part to the failure to correctly account for turbulence associated with Langmuir circulations. They concluded that there is a pressing need for more microstructure measurements within the ocean surface boundary layer. Our results support this assessment, by indicating that there may still be other processes contributing significantly to near-surface mixing that have yet to be accounted for.

**Acknowledgments.** D. Wain was supported at the National University of Ireland, Galway by the European Space Agency under ESRIN/Contract No. 4000102925/11/I-AM, and by Irish Research Council grant EPSPD/2011/218. J. Lilly was supported by Award OCE-1036097 from the Physical Oceanography program of the United States National Science Foundation; this grant also supported the 2010 ASIP deployment and subsequent data processing. B. Ward acknowledges support from Science Foundation Ireland under Grant 08/US/I1455 and the NUIG Millenium fund (RM0908). A. Callaghan acknowledges funding from the Irish Research Council Marie Curie INSPIRE fellowship. We thank the Bedford Institute of Oceanography for graciously providing the necessary ship time, and Chief Scientist Glen Harrison for prioritizing the ASIP measurements. We also extend our thanks to the captain and crew of the CCGS Hudson for making this study possible, and in particular to first officer Douglas Roe, who piloted the ship's Fast Rescue Craft during the ASIP deployments and recoveries. We also would like to thank the

three reviewers for their helpful suggestions for improving this manuscript. Any requests concerning the data in this paper should be directed to Jonathan Lilly at [lilly@nwra.com](mailto:lilly@nwra.com).

## References

- Alford, M. H., and R. Pinkel (2000), Observations of overturning in the thermocline: The context of ocean mixing, *J. Phys. Oceanogr.*, *30.5*, 805–832.
- Ansong, J. K., and B. R. Sutherland (2010), Internal gravity waves generated by convective plumes, *J. Fluid Mech.*, *648*, 405–434.
- Barad, M. F., and O. B. Fringer (2010), Simulations of shear instabilities in interfacial gravity waves, *J. Fluid Mech.*, *644*, 61–95, doi:10.1016/S0079-6611(01)00069-6.
- Barton, E. D., M. E. Inall, T. J. Sherwin, and R. Torres (2001), Vertical structure, turbulent mixing and fluxes during Lagrangian observations of an upwelling filament system off Northwest Iberia, *Prog. Oceanogr.*, *51*(2-4), 249–267, doi:10.1016/S0079-6611(01)00069-6.
- Belcher, S. E., A. L. M. Grant, K. E. Hanley, B. Fox-Kemper, L. Van Roekel, P. P. Sullivan, W. G. Large, A. Brown, A. Hines, D. Calvert, A. Rutgersson, H. Pettersson, J.-R. Bidlot, P. A. E. M. Janssen, and J. A. Polton (2012), A global perspective on Langmuir turbulence in the ocean surface boundary layer, *Geophys. Res. Lett.*, *39*(18), L18,605–1–9, doi:10.1029/2012GL052932.
- Bell, T. H. (1978), Radiation damping of inertial oscillations in the upper ocean, *J. Fluid Mech.*, *88*, 289–308, doi:10.1017/S0022112078002116.
- Callaghan, A. H., B. Ward, and J. Vialard (2014), Influence of surface forcing on near-surface and mixing layer turbulence in the tropical Indian Ocean, *Deep-Sea Res. I*, *94*,

107–123, doi:10.1016/j.dsr.2014.08.009.

Dewey, R., R. Muench, and J. Gunn (1999), Mixing and vertical heat flux estimates in the Arctic Eurasian Basin, *J. Mar. Syst.*, *21*(1-4), 199–205, doi:10.1016/S0924-7963(99)00014-7, 29th International Liege Colloquium on Ocean Hydrodynamics, LIEGE, BELGIUM, MAY 05-09, 1997.

Dohan, K., and R. E. Davis (2011), Mixing in the transition layer during two storm events, *J. Phys. Oceanogr.*, *41*, 42–66.

Dohan, K., and B. R. Sutherland (2003), Internal waves generated from a turbulent mixed region, *Phys. Fluids*, *15*(2), 488–498, doi:10.1063/1.1530159.

Fox-Kemper, B., G. Danabasoglu, R. Ferrari, S. M. Griffies, R. W. Hallberg, M. M. Holland, M. E. Maltrud, S. Peacock, and B. L. Samuels (2011), Parameterization of mixed layer eddies. III: Implementation and impact in global ocean climate simulations, *Ocean Modell.*, *39*(1–2), 61–78.

Fringer, O., and R. Street (2003), The dynamics of breaking progressive interfacial waves, *J. Fluid Mech.*, *494*, 319–353, doi:10.1017/S0022112003006189.

Gill, A. E. (1982), *Atmosphere—Ocean Dynamics*, 662 pp., Academic Press.

Johnston, T. M. S., and D. L. Rudnick (2009), Observations of the Transition Layer, *J. Phys. Oceanogr.*, *39*(3), 780–797, doi:10.1175/2008JPO3824.1.

Joyce, T. M., and M. C. Stalcup (1984), An upper ocean current jet and internal waves in a Gulf Stream warm core ring, *J. Geophys. Res.*, *89*(C2), 1997–2003.

Kundu, P. K., and I. M. Cohen (2002), *Fluid Mechanics*, Academic Press.

Lauderdale, J. M., S. Bacon, A. C. N. Garabato, and N. P. Holliday (2008), Intensified turbulent mixing in the boundary current system of southern Greenland, *Geophys. Res.*

*Lett.*, 35(4), doi:10.1029/2007GL032785.

Lazier, J., R. Hendry, A. Clarke, I. Yashayaev, and P. Rhines (2002), Convection and restratification in the Labrador Sea, 1990-2000, *Deep Sea Res. I*, 49(10), 1819–1835, doi:10.1016/S0967-0637(02)00064-X.

Lien, R. C., E. A. D’Asaro, and M. J. McPhaden (2002), Internal waves and turbulence in the upper central equatorial Pacific: Lagrangian and Eulerian observations, *J. Phys. Oceanogr.*, 32(9), 2619–2639, doi:10.1175/1520-0485-32.9.2619.

Lilly, J. M., P. B. Rhines, M. Visbeck, R. Davis, J. R. Lazier, F. Schott, and D. Farmer (1999), Observing deep convection in the Labrador Sea during winter 1994–1995, *J. Phys. Oceanogr.*, 29, 2065–2098.

Marshall, J., and F. Schott (1999), Open-ocean convection: observations, theory and models, *Rev. Geophys.*, 37(1), 1–64.

McDougall, T., and P. Barker (2011), *Getting started with TEOS-10 and the Gibbs Seawater (GSW) Oceanographic Toolbox*, SCOR/IAPSO WG127.

Moum, J. N., D. M. Farmer, W. D. Smyth, L. Armi, and S. Vagle (2003), Structure and generation of turbulence at interfaces strained by internal solitary waves propagating shoreward over the continental shelf, *J. Phys. Oceanogr.*, 33, 2093–2112.

Oakey, N. S. (1982), Determination of the rate of dissipation of turbulent energy from simultaneous temperature and velocity shear microstructure measurements, *J. Phys. Oceanogr.*, 12(3), 256–271, doi:10.1175/1520-0485(1982)012.

Osborn, T. (1980), Estimates of the local rate of vertical diffusion from dissipation measurements, *J. Phys. Oceanogr.*, 10, 83–89.

- Peterson, B. J., J. McClelland, R. Curry, R. M. Holmes, J. E. Walsh, and K. Aagaard (2006), Trajectory shifts in the Arctic and subarctic freshwater cycle, *Science*, *313*(5790), 1061–1066.
- Polton, J. A., J. A. Smith, J. A. MacKinnon, and A. E. Tejada-Martinez (2008), Rapid generation of high-frequency internal waves beneath a wind and wave forced oceanic surface mixed layer, *Geophys. Res. Lett.*, *35*(13), doi:10.1029/2008GL033856.
- Polzin, K. L., and Y. V. L’vov (2011), Toward regional characterizations of the oceanic internal wavefield, *Rev. Geophys.*, *49*, 2010RG000,329 (1–61).
- Schmidt, S., and U. Send (2007), Origin and composition of seasonal Labrador Sea freshwater, *J. Phys. Oceanogr.*, *37*, 1445–1454.
- Simmons, H. L., and M. H. Alford (2012), Simulating the long-range swell of internal waves generated by ocean storms, *Oceanogr.*, *25*(2), 30–41.
- Smyth, W. L., and K. B. Winters (2003), Turbulence and mixing in Holmboe waves, *J. Phys. Oceanogr.*, *33*(4), 694–711.
- Stevens, C., B. Ward, C. S. Law, and M. Walkington (2011), Surface layer mixing during the SAGE ocean fertilization experiment, *Deep-Sea Res.*, *58*, 776–787.
- Straneo, F. (2006), Heat and freshwater transport through the central Labrador Sea, *J. Phys. Oceanogr.*, *36*(4), 606–628.
- Sutherland, G., K. H. Christensen, and B. Ward (2013), Wave-turbulence scaling in the ocean mixed layer, *Ocean Sci.*, *9*, 597–608, doi:10.5194/os-9-597-2013.
- Sutherland, G., K. H. Christensen, and B. Ward (2014), Evaluating langmuir turbulence in the ocean surface boundary layer, *J. Geophys. Res.*, doi:10.1002/2013JC009537.

- Thorpe, S. (1978), Shape and breaking of finite-amplitude internal gravity-waves in a shear-flow, *J. Fluid Mech.*, *85*(MAR), 7–32, doi:10.1017/S0022112078000518.
- Thorpe, S. A. (2005), *The Turbulent Ocean*, Cambridge University Press.
- Troy, C., and J. Koseff (2005), The instability and breaking of long internal waves, *J. Fluid Mech.*, *543*, 107–136, doi:10.1017/S0022112005006798.
- Våge, K., R. S. Pickart, V. Thierry, G. Reverdin, C. M. Lee, B. Petrie, T. A. Agnew, A. Wong, and M. H. Ribergaard (2009), Surprising return of deep convection to the subpolar north atlantic ocean in winter 2007–2008, *Nat. Geosci.*, *2*(1), 67–72.
- Walter, M., C. Mertens, and M. Rhein (2005), Mixing estimates from a large-scale hydrographic survey in the North Atlantic, *Geophys. Res. Lett.*, *32*(13), doi:10.1029/2005GL022471.
- Ward, B., T. Fristedt, A. H. Callaghan, G. Sutherland, X. Sanchez, and J. Vialard (2014), The Air-Sea Interaction Profiler (ASIP): An autonomous upwardly-rising profiler for microstructure measurements in the upper ocean, *J. Atmos. Oceanic Technol.*, *31*, 2246–2267, doi:10.1175/JTECH-D-14-00010.1.
- Wijesekera, H. W., and T. M. Dillon (1991), Internal waves and mixing in the upper equatorial Pacific Ocean, *J. Geophys. Res.*, *96*(C4), 7115–7125, doi:10.1029/90JC02727.
- Yamazaki, H., and T. R. Osborn (1990), Dissipation estimates for stratified turbulence, *J. Geophys. Res.*, *95*, 97399744.
- Yashayaev, I. (2007), Hydrographic changes in the Labrador Sea, 1960-2005, *Prog. Oceanogr.*, *73*(3-4), 242–276, doi:10.1016/j.pocean.2007.04.015.
- Yashayaev, I., and J. W. Loder (2009), Enhanced production of Labrador Sea Water in 2008, *Geophys. Res. Lett.*, *36*, doi:10.1029/2008GL036162.

Accepted Article

**Figure 1.** Bathymetric map of the Labrador Sea with primary currents labeled. The position of the CTD casts from the 2010 survey of the AR7W line are indicated by filled white circles. The profiles used to create the transect in Figure 2 are highlighted in purple.

D R A F T

May 2, 2015, 7:45pm

D R A F T



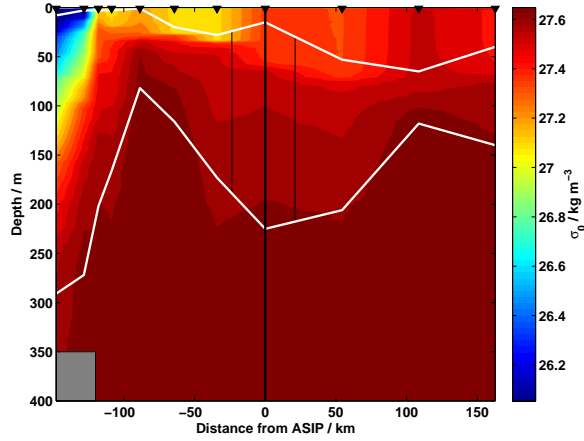


**Figure 2.** Density section across the upper 350 m of the western portion of the AR7W transect, corresponding the portion highlighted in purple in Figure 1. The black triangles indicate the location of the CTD casts. The envelope of  $N$  equal to the frequency of the observed waves is indicated by white lines, which therefore delimit the upper and lower boundaries of the ray paths. The thick vertical black line indicates the approximate position of the ASIP measurements, and the distances on the  $x$ -axis are computed relative to this point. The thin black line is the horizontal distance that a wave of this frequency would travel in 100 reflections off the boundaries of the  $N$  envelope. The grey box in the lower left is due to a decrease in bottom depth approaching the continental slope.

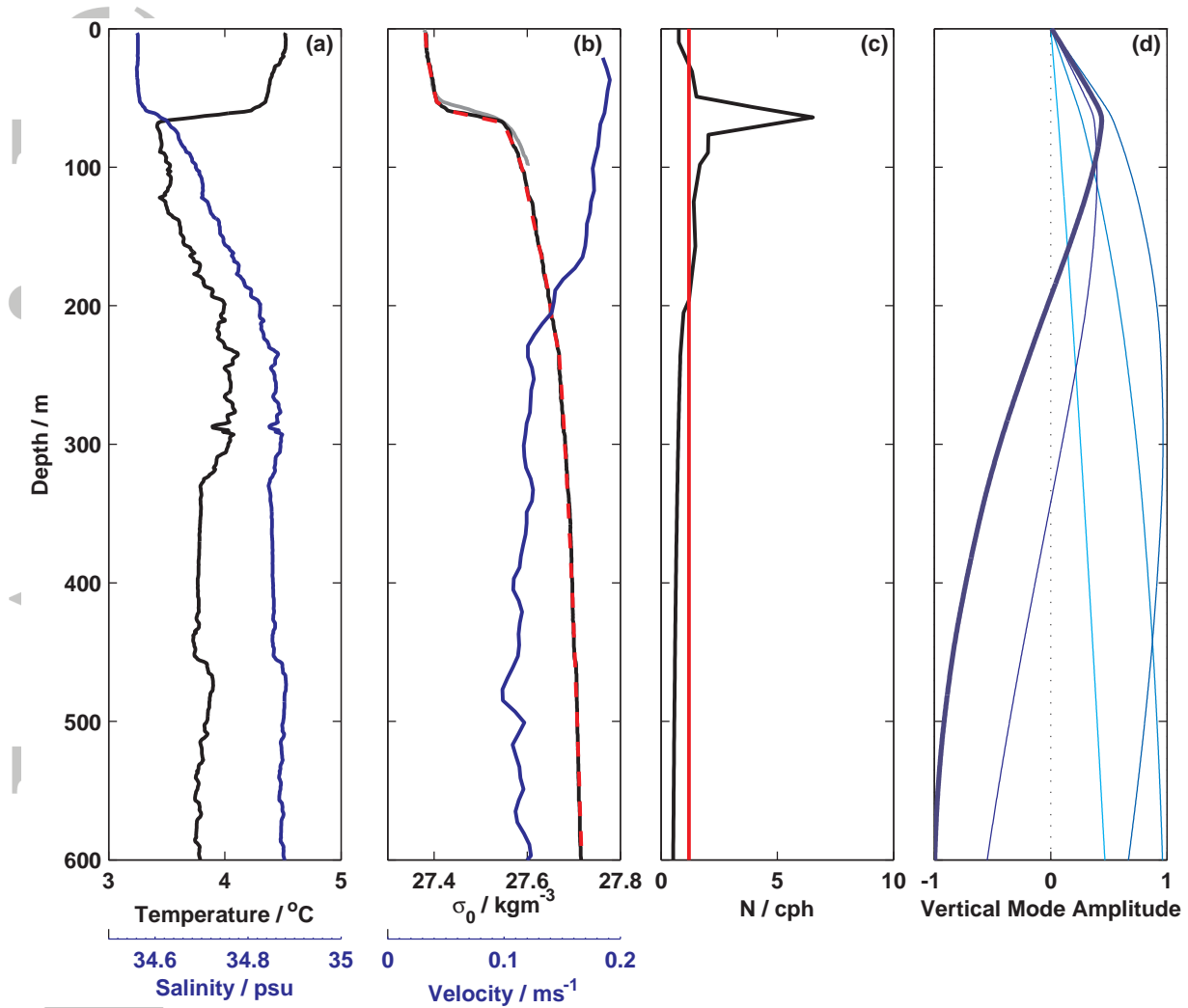


**Figure 3.** (a) Temperature and salinity profiles from the shipboard CTD cast concurrent with the ASIP measurements. (b) Density profile from the CTD, together with velocity magnitude from the shipboard ADCP. The piecewise linear fit to the density profile is shown as a red dashed line overlying the original data. The mean ASIP density profile is shown in grey. (c) Buoyancy frequency profile. The vertical red line indicates the estimated frequency— $0.002 \text{ rad s}^{-1}$ , or a 50 minute period—of the internal wave. (d) The upper 600 m of the vertical structure functions for the first five vertical modes, with mode one in the lightest color and proceeding to mode five in the darkest color. Mode five is indicated as a heavy line.

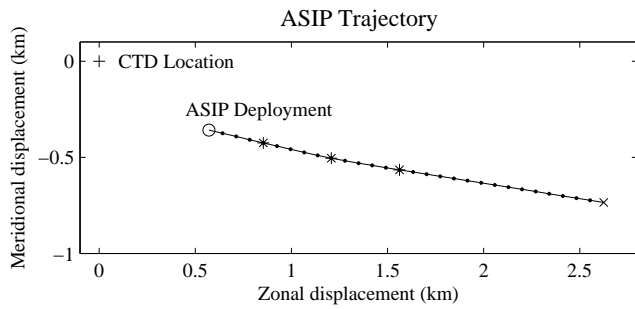


**Figure 4.** The estimated trajectory of ASIP relative to the CTD cast, indicated by a “+”, during the deployment on 22 May 2010. ASIP was deployed from a small boat about a kilometer away from the *Hudson* at the location marked by a circle. Note that only the three points marked by asterisks are based on valid GPS fixes; the dots are estimated locations based on interpolating or extrapolating the velocities from the valid points.

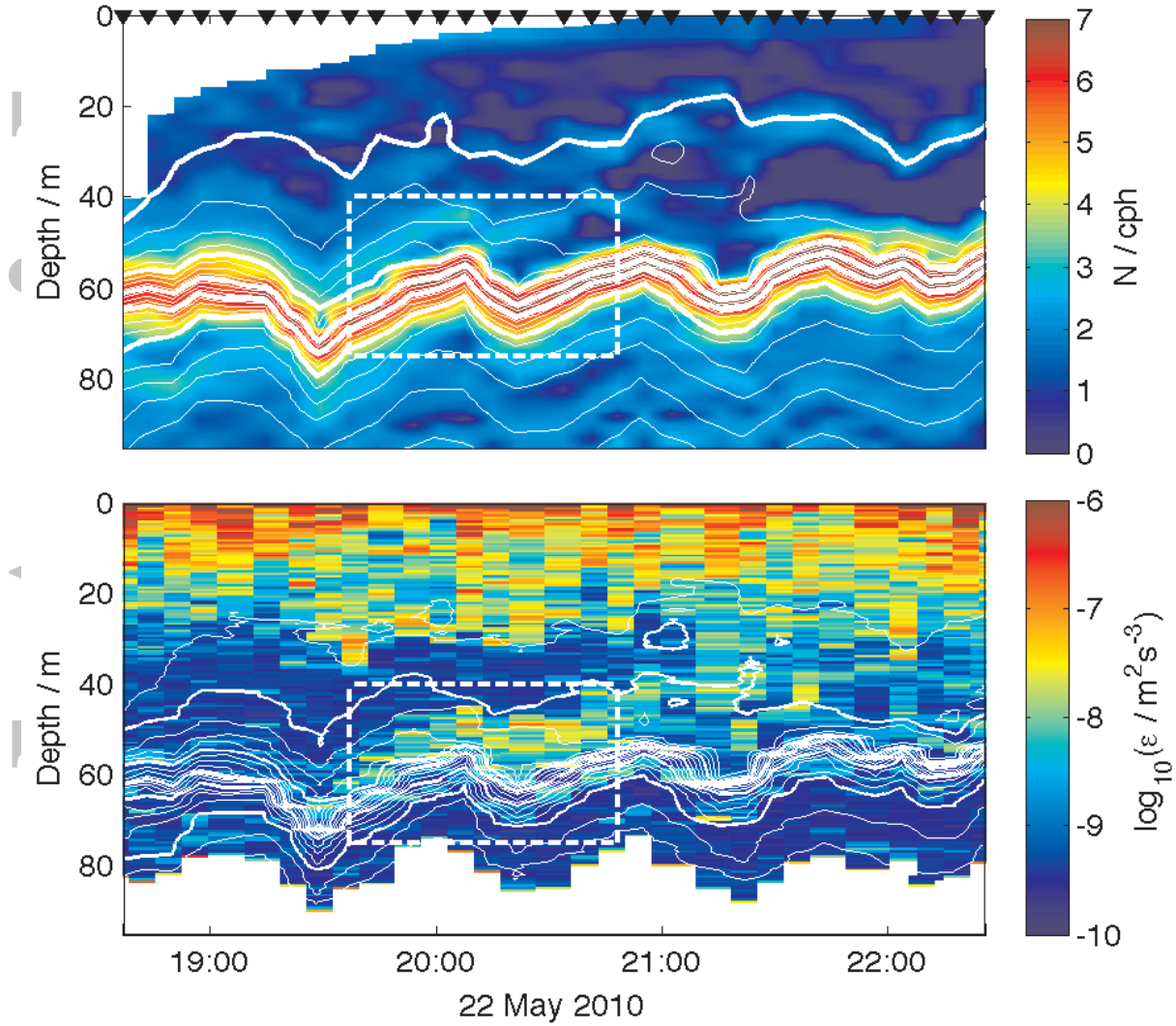


**Figure 5.** Four-hour records of: (a) Buoyancy frequency  $N$  overlaid by the isopycnals of the smoothed density profiles. (b) Dissipation rate of turbulent kinetic energy  $\epsilon$  overlaid by the isopycnals from the unsmoothed density profiles. The time of the profiles is marked by the black triangles. All isopycnals (white lines) are spaced at  $0.01 \text{ kg m}^{-3}$  intervals. The isopycnals used to determine the profile in Figure 7 are highlighted. The elevated dissipation due to the breaking internal wave is demarcated by the dashed box.

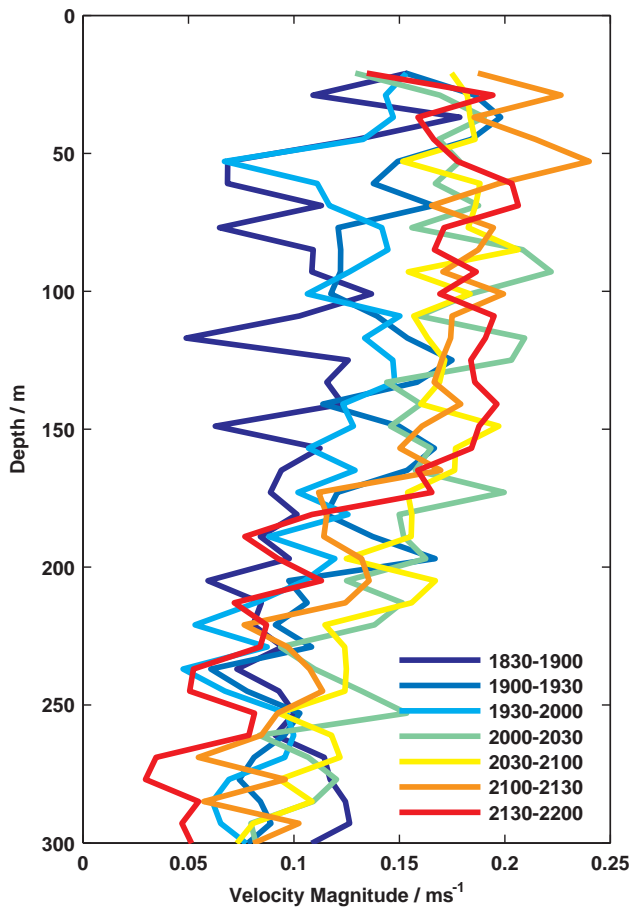


**Figure 6.** 30 minute averages of the velocity magnitude measured by the shipboard ADCP.

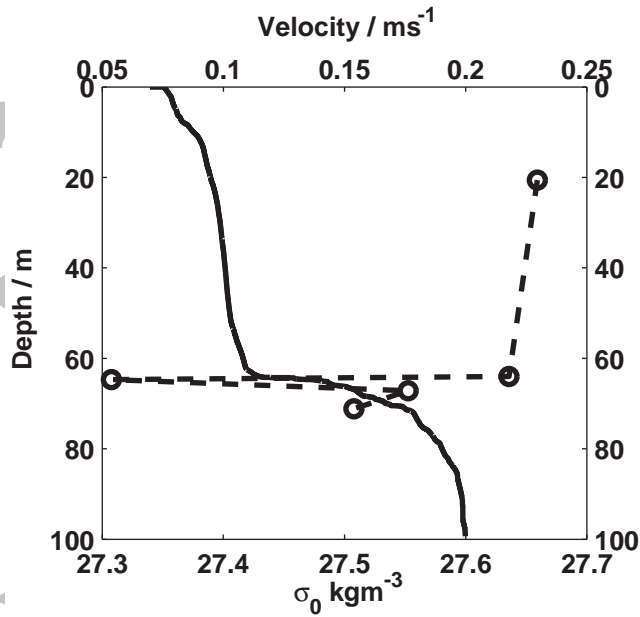


**Figure 7.** Sorted density profile (solid line) from Profile 10 (measured at 19:43) and inferred velocity profile (dashed line) following the method set forth in *Moum et al.* [2003].

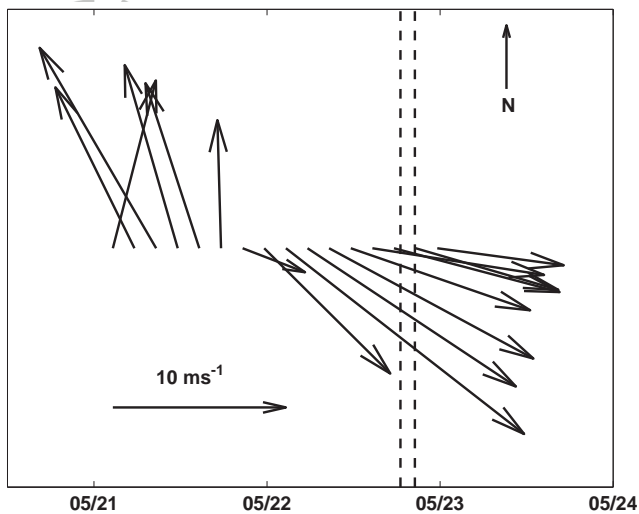


**Figure 8.** Wind speed and direction from ECMWF at the position of ASIP before and during the deployment.